*J. Fluid Mech.* (1995), *vol.* 284, *pp.* 225–237



# The time-dependent free surface flow induced by a submerged line source or sink

By E. M. SOZER AND M. D. GREENBERG
Department of Mechanical Engineering, University of Delaware, Newark, DE 19716, USA

(Received 4 May 1994 and in revised form 7 September 1994)

The unsteady nonlinear potential flow induced by a submerged line source or sink is studied by a vortex sheet method, both to trace the free surface evolution and to explore the possible existence of steady-state solutions. Only steady-state flows have been considered by other investigators, and these flows have been insensitive to whether they are generated by a source or sink, except with respect to the flow direction along the streamlines. The time-dependent solution permits an assessment of the stability of previously found steady solutions, and also reveals differences between source and sink flows: for the infinite-depth case, steady stagnation-point-type solutions are found for source flows, even above the critical value of source/sink strength reported by other investigators; for the finite-depth case, steady stagnation-point-type solutions are found both for source flows and sink flows, above the critical value reported by other investigators; finally, it is shown that streamline patterns of steady stagnation-point flows are identical for source and sink flows only in the limiting case of infinite depth.

## 1. Introduction

The nonlinear potential flow induced by a line source or sink below a free surface has attracted interest not only as a fundamental problem but also in connection with the selective withdrawal of fluid from a reservoir, a cooling pond for a power station, or a solar pond for energy conversion. The steady-state case has been studied by perturbation and function-theoretic methods (Hocking 1985, 1991; Forbes & Hocking 1993; Hocking & Forbes 1991, 1992; Vanden-Broeck, Schwartz & Tuck 1978; Vanden-Broeck & Keller 1987; Tuck & Vanden-Broeck 1984), and striking results have been obtained. For the case of infinite-depth fluid, Vanden-Broeck *et al.* (1978) showed that the series expansion of the free surface elevation in the Froude number $F$ (non-dimensional source/sink strength) proceeds in even powers of $F$, so that the free surface shape and streamlines are insensitive to whether the singularity is a source or sink (although the directions of flow along the streamlines are opposite for the two cases). The solution obtained by them has been called a *stagnation-point flow* because it is characterized by a stagnation point at the free surface, directly above the source/sink. Motivated by the way the free surface shape evolves as $F$ is increased, and by studies of stratified fluids, Tuck & Vanden-Broeck (1984) sought cusp-like solutions, where the free surface shape is a downward facing cusp with its tip above the source/sink. They found that such a solution could be obtained only if $F^2$ were included as one of the unknowns, and a *cusp* solution was indeed found at a unique value of $F^2$. Numerous stagnation-point solutions (Hocking & Forbes 1991, 1992; Peregrine 1972; Vanden-Broeck & Keller 1987; Vanden Broeck *et al.* 1978) and cusp

solutions (Craya 1949; Hocking 1985, 1991; Tuck & Vanden-Broeck 1984; Vanden-Broeck & Keller 1987) can now be found in the literature.

For the infinite-depth case, the stagnation-point solutions are reported only for $0 \leqslant |F| < |F_{cr}| = 1.42$. Above that critical value, steady-state solutions have not been found, except for a cusp solution at the unique supercritical value $|F| = 3.55$.

For the finite-depth case, two critical values are reported, rather than one. For $0 \leqslant |F| < |F_{cr1}|$ stagnation-point solutions are reported, for $|F_{cr1}| < |F| < |F_{cr2}|$ no steady solutions are obtained, and cusp flows are found for all $|F|$ above $|F_{cr2}|$. $F_{cr1}$ and $F_{cr2}$ are functions of the ratio of the water depth to the source/sink depth. They are approximately 0.23 and 1.0, respectively, when the depth ratio is unity (Hocking & Forbes 1992).

To shed additional light on these flow regimes for the infinite-depth case Sozer (1994) and Sozer & Greenberg (1993) studied the *unsteady* flow and approach to steady state by applying a vortex sheet approach that was developed by Zaroodny & Greenberg (1973) and developed independently by Baker, Meiron & Orszag (1982). For representative subcritical Froude numbers (i.e. below 1.42), a stable approach to the stagnation-point solution was found. For the source case, stable stagnation-point solutions were found, for the first time, for Froude numbers greater than 1.42 as well. In the present paper we extend those results and also consider the case of finite depth.

## 2. Vortex sheet approach

It is known from classical potential theory that the potential flow in the air (i.e. the fluid above the free surface) can be generated by a vortex sheet along the free surface, and that the potential flow in the water (i.e. the fluid between the free surface and bottom) can be generated by a different vortex sheet along the free surface together with the source/sink and an image system below the bottom. However, it is simpler to generate both flows by the same free surface vortex sheet, source/sink, and their image system since such a system automatically satisfies the kinematic free surface boundary condition that the normal velocity is continuous across the free surface. This arrangement is shown in figure 1, where the $x$-axis coincides with the undisturbed water level, $Q$ is the source/sink strength (positive for source, negative for sink), $Y(x, t)$ is the free surface elevation, $G(x, t)$ is the free surface vortex density (circulation per unit $x$-length), and $t$ is the time.

As derived in Sozer (1994) and Sozer & Greenberg (1993), the evolution equations governing $Y$ and $G$ are

$$Y_t = V - UY_x, \tag{2.1}$$

$$G_t = -(UG)_x + \tfrac{1}{2}\kappa[C^2 G(CSGY_{xx} - G_x) - 4(U_t + UU_x) - 4(V_t + UV_x + 1)\,Y_x] + \frac{2\tau}{\rho^a + \rho^w}\left[\frac{Y_{xx}}{(1+Y_x^2)^{3/2}}\right]_x, \tag{2.2}$$

where subscripts denote partial derivatives; $\kappa = (\rho^w - \rho^a)/(\rho^w + \rho^a)$ with $\rho^a$ and $\rho^w$ the densities of air and water, respectively; $\tau$ is the surface tension; $S \equiv \sin(\tan^{-1} Y_x) = Y_x/(1+Y_x^2)^{1/2}$ and $C \equiv \cos(\tan^{-1} Y_x) = 1/(1+Y_x^2)^{1/2}$; and $U$, $V$ are the averaged $x, y$ velocities at the free surface, $U = \frac{1}{2}(u^a + u^w)$ and $V = \frac{1}{2}(v^a + v^w)$. Equation (2.1) expresses the kinematic condition that particles once on the free surface remain on the free surface, and equation (2.2) expresses the dynamic condition that the pressure jump across the free surface is due to the interaction of surface tension and free surface curvature. In this study we take $\tau = 0$. Lengths, velocities, and time have been non-

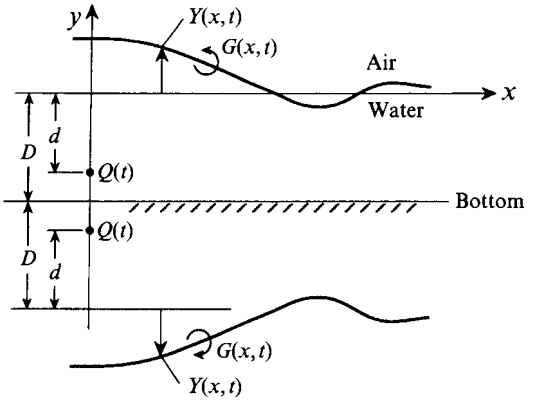


FIGURE 1. Vortex system geometry.

dimensionalized with respect to $d$, $(gd)^{1/2}$, and $(d/g)^{1/2}$, respectively, where $g$ is the acceleration due to gravity. Also,

$$U(x,t) = \frac{FH(t)}{2\pi}\left\{\frac{x}{x^2+[1+Y(x,t)]^2}+\frac{x}{x^2+[2a-1+Y(x,t)]^2}\right\}$$
$$+\frac{1}{2\pi}\int_{-\infty}^{\infty}\left\{\frac{Y(\xi,t)-Y(x,t)}{(\xi-x)^2+[Y(\xi,t)-Y(x,t)]^2}+\frac{2a+Y(\xi,t)+Y(x,t)}{(\xi-x)^2+[2a+Y(\xi,t)+Y(x,t)]^2}\right\}G(\xi,t)\,\mathrm{d}\xi, \tag{2.3a}$$

$$V(x,t) = \frac{FH(t)}{2\pi}\left\{\frac{1+Y(x,t)}{x^2+[1+Y(x,t)]^2}+\frac{2a-1+Y(x,t)}{x^2+[2a-1+Y(x,t)]^2}\right\}$$
$$-\frac{1}{2\pi}\int_{-\infty}^{\infty}\left\{\frac{\xi-x}{(\xi-x)^2+[Y(\xi,t)-Y(x,t)]^2}-\frac{\xi-x}{(\xi-x)^2+[2a+Y(\xi,t)+Y(x,t)]^2}\right\}G(\xi,t)\,\mathrm{d}\xi, \tag{2.3b}$$

where $F = Q/(gd^3)^{1/2}$ is the Froude number, $H(t)$ is a Heaviside step function, and $a = D/d$ is the depth ratio.

It can be verified that (2.1)–(2.3) are equivalent to the analogous equations in Baker *et al.* (1982) although Baker *et al.* use complex variable notation, doublets rather than vortices (one can transform from doublets to vortices by integration by parts), a Lagrangian scheme rather than Eulerian, and assumes periodicity in the $x$-direction. Note that if the air density is zero, as assumed in the other papers on this problem, then $\kappa = 1$, whereas if the air density is accounted for then $\kappa$ is slightly less than 1. Thus, the vortex model allows for superposed fluids without complication. The only significant simplification of the system (2.1)–(2.3) would be for the case of internal waves, where $\kappa = 0$.

## 3. Numerical solution

Equations (2.1)–(2.3) comprise a set of nonlinear, Cauchy-singular integro-differential equations for $Y(x,t)$ and $G(x,t)$, to which we add the initial conditions $Y(x,0) = G(x,0) = 0$. The integrals are of Cauchy principal value type, but are desingularized by 'folding' the $\xi$-axis about the computation point $x$, to allow the positive and negative singularities to cancel. To handle the infinite extent of the inte-

gration domain, the asymptotic approximations $G(x,t) = A_1/x + A_2/x^3$ and $Y(x,t) = A_3/x^2 + A_4/x^4$ are used in the 'tails' from the ends of the computational domain to infinity, where the constants $A_1$–$A_4$ are computed at each time step by means of a least-squares fit over the last several computational points. These forms are suggested by the asymptotic behaviour of the perturbation solutions given below in §4.1. Fourth-order Simpson's integration is used in the finite computational domain, and the tail integrals are calculated analytically. Within the computational domain, a uniform spacing of $\Delta x = 0.1$ is used between nodal points, that spacing being sufficiently small to resolve the $Y$ and $G$ forms that result. (Reducing $\Delta x$ to 0.05 and 0.025 results in plots of $Y$ and $G$ that are indistinguishable from those corresponding to $\Delta x = 0.1$.)

Fourth-order Runge–Kutta integration is used for the time integration, but that calculation is complicated by the $U_t$ and $V_t$ terms in (2.2) since they contain $G_t$ within the $\xi$-integrals. Following Zaroodny & Greenberg (1973), we use an iterative procedure to handle those terms, with the initial estimate of $G_t$ (in $U_t$ and $V_t$) based upon an extrapolation from previous time steps. Essentially the same procedure was adopted in Baker *et al.* (1982) and those authors proved the convergence of the iteration. Their proof is unaffected by the presence of the source/sink and its image.

We approximate $H(t)$ in (2.3) as $\sin(500\pi t)$ from $t = 0$ to 0.001, and unity for $t > 0.001$. Ten equal time steps are used from $t = 0$ to 0.001, after which we computed at $t = 0.1$, 0.2, and so on.

A numerical instability arises in all the variables $Y$, $G$, $U$ and $V$, and is unrelated to the handling of the 'tail' regions since its onset is independent of the size of the computational domain. This instability was also observed by Baker *et al.* (1982), who used periodic boundary conditions in the $x$-direction, and Telste (1987), who used 'sponge layers' at the ends of the $x$-computational domain. To suppress the instability, linear filtering is used, as in Telste. Specifically, a five-point smoothing formula is applied at all nodal points except for two points at each end of the computational domain. These four points are handled by extrapolating from the adjacent points. The five-point smoothing formula (Longuet-Higgins & Cokelet 1976; Shapiro 1975) is

$$W_i^{new} = \tfrac{1}{16}(-W_{i-2}^{old} + 4W_{i-1}^{old} + 10W_i^{old} + 4W_{i+1}^{old} - W_{i+2}^{old}), \tag{3.1}$$

where $W_i$ represents $Y$, $G$, $U$ or $V$ at a fixed $t$ and at the $i$th nodal point. As in Telste (1987), filtering is applied after each time step.

## 4. Infinite-depth limit

### 4.1. *Perturbation solution*

For comparison with our numerical results, we also consider a perturbation solution in the Froude number $F$. Of special interest is the steady state, for which we seek $Y(x) = FY_1(x) + F^2Y_2(x) + \ldots$, and similarly for $G(x)$, $U(x)$, and $V(x)$. This case was treated in (Sozer 1994), and it was found that

$$G(x) = F\frac{1}{\pi}\frac{x}{x^2+1} - F^3\frac{3(\kappa+1)}{16\pi^3\kappa}\frac{x(x^4-6x^2+1)}{(x^2+1)^4} + O(F^5), \tag{4.1a}$$

$$Y(x) = -F^2\frac{\kappa+1}{4\pi^2\kappa}\left(\frac{x}{x^2+1}\right)^2 + F^4\frac{3(\kappa+1)^2}{32\pi^4\kappa^2}\frac{x^2(x^4-6x^2+1)}{(x^2+1)^5} + O(F^6). \tag{4.1b}$$

For $\kappa = 1$ this $Y(x)$ is in agreement with results given in Vanden-Broeck *et al.* (1978), wherein the air density was taken to be zero. ($G(x)$ was not found in Vanden-Broeck

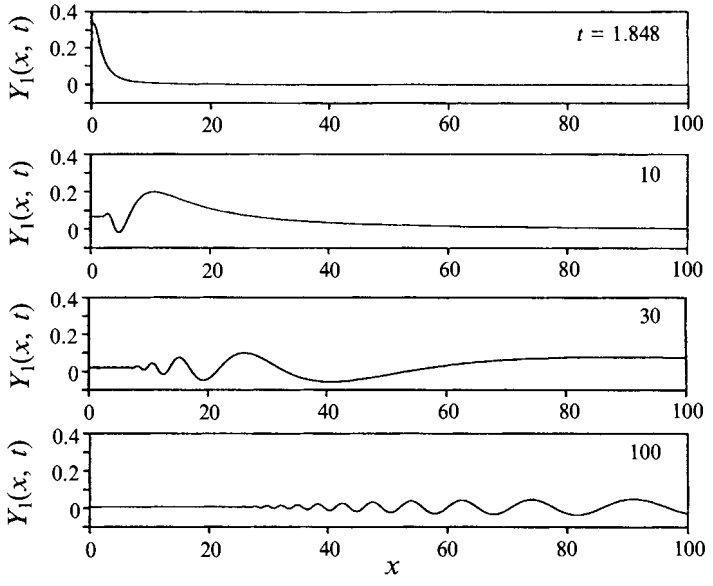


FIGURE 2. $Y_1(x, t)$ evolution for $\kappa = 1$; infinite-depth case.

*et al.* since those authors did not use a vortex sheet model.) Equations (4.1*a*, *b*) correspond to the stagnation point solution and, as noted above, the free surface shape is insensitive to the sign of $Q$ (and hence $F$) since the expansion proceeds in even powers of $F$.

For the unsteady case we seek

$$Y(x, t) = FY_1(x, t) + F^2 Y_2(x, t) + \ldots \tag{4.2}$$

and similarly for $G(x, t)$, $U(x, t)$, and $V(x, t)$. As shown in Sozer (1994) and Sozer & Greenberg (1993)

$$Y_1(x, t) = \frac{1+\kappa}{2\pi\kappa^{1/2}} \int_0^\infty \frac{e^{-w} \cos(xw) \sin(t(\kappa w)^{1/2})}{w^{1/2}} dw, \tag{4.3a}$$

$$G_1(x, t) = \frac{1}{\pi} \frac{x}{x^2+1} - \frac{1+\kappa}{\pi} \int_0^\infty e^{-w} \sin(xw) \cos(t \to (\kappa w)^{1/2}) dw, \tag{4.3b}$$

which do tend to the correct steady-state values 0 and $x/\pi(x^2+1)$ respectively, as $t \to \infty$. In particular, for $x = 0$ and $\kappa = 1$

$$Y_1(0, t) = \frac{2}{\pi} e^{-t^2/4} \int_0^{t/2} e^{\eta^2} d\eta \tag{4.4}$$

is a tabulated Dawson's integral (Abramowitz & Stegun 1964, p. 298). $Y_1(0, t)$ increases from zero to a maximum of 0.34443945 at $t = 1.8482777$, then decreases monotonically to zero as $t \to \infty$. In fact, $Y_1(x, t)$ exhibits a rather flat interval centred at $x = 0$, that broadens with time, as seen in figure 2. (We choose $\kappa = 1$, in our calculations, for comparison with other papers that take the air density to be zero.)

The computational domain is chosen to be $-200 < x < 200$. In view of the algebraic decay forms used for $G$ and $Y$ in the 'tails', it seems prudent to terminate the calculation before the inflection point to the right of the outermost crest reaches the

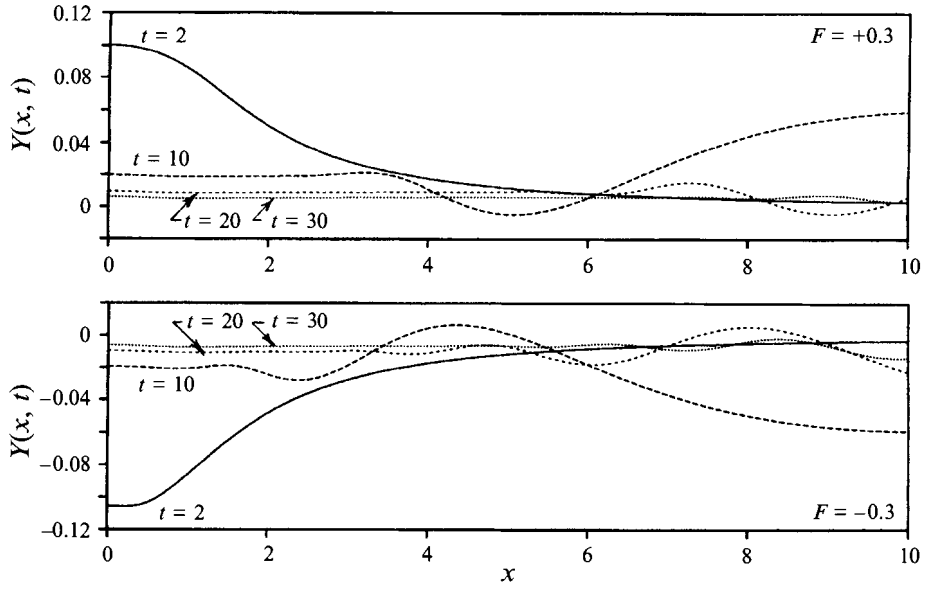


FIGURE 3. $Y(x,t)$ induced by $F = \pm 0.3$.

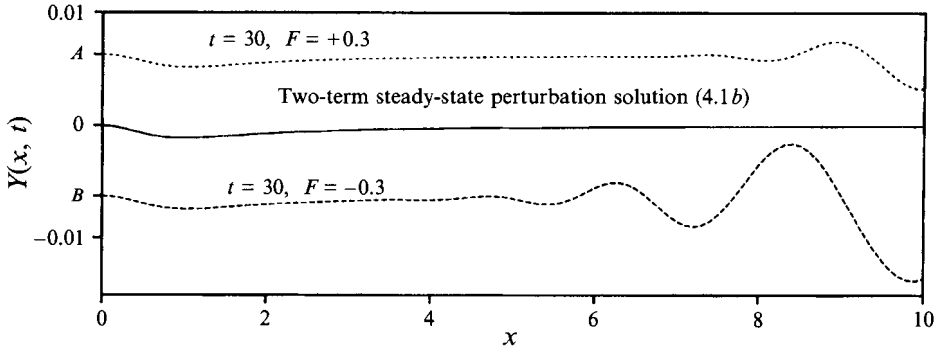


FIGURE 4. Blow-up of figure 3, for $t = 30$.

end of the computational domain. With that limit in mind, calculations are carried as far as $t = 30$ for this choice of computational domain.

### 4.2. *Numerical results*

As noted in the introduction, stagnation point solutions have been obtained in the literature only for $|F|$ below some critical value, namely, $|F| < |F_{cr}| \approx 1.42$. As a first case, consider the subcritical values $F = \pm 0.3$. The computed free surface elevation $Y(x,t)$ is shown in figures 3 and 4 for representative times until $t = 30$. We see that the free surface does indeed approach the steady-state stagnation point solution (more specifically, the two-term perturbation solution (4.1*b*)). The approach to steady state, displayed in figure 4, is even more compelling if we notice that the difference between the $t = 30$ free surface shapes and the two-term perturbation solution are essentially constants over $0 \leqslant x \lesssim 5$, and that difference is due primarily to the $FY_1(x,t)$ term in the unsteady perturbation solution (4.2), which is quite flat at $t = 30$ over $0 \leqslant x \lesssim 5$ (figure 2). (For instance, $A = 0.006273$ and $B = -0.006226$ whereas $FY_1(0,30) =$

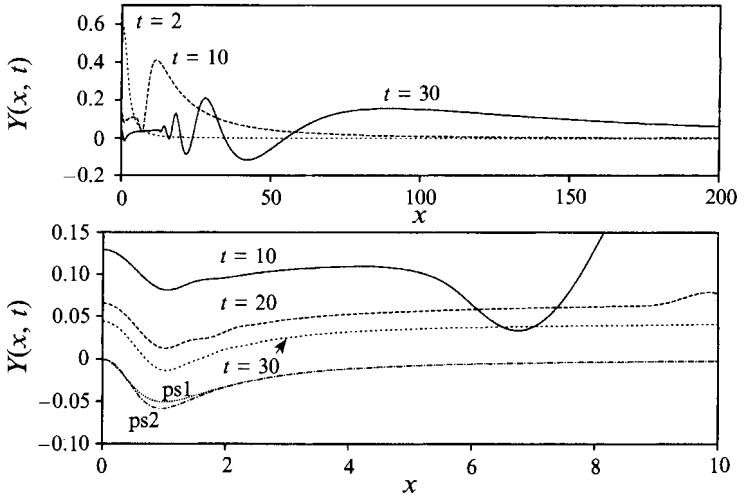


FIGURE 5. $Y(x, t)$ evolution, for $F = +2$.

$\pm 0.3 Y_1(0, 30) = \pm 0.006381$.) Since the $Y_1(x, t)$ 'plateau' tends monotonically to zero (figure 2), we can infer that the dashed curves in figure 4 will continue to approach the two-term steady-state perturbation solution as $t$ increases.

An indirect assessment of the accuracy of the numerical results was carried out as follows. The program was run, up to $t = 10$, for the six cases $F = \pm 0.1, \pm 0.2, \pm 0.3$. Equation (4.2) was written out for each of these cases, each time with a known (i.e. computed) function $Y(x, t)$ on the left-hand side. From these six equations, $Y_1(x, t)$ was found, by algebra, to within an error of $O(F^6)$. Since $Y_1(x, t)$ is known exactly (i.e. analytically), this procedure permitted an indirect assessment of the accuracy. The maximum percent error,

$$100 \frac{\text{calculated } Y_1(x, t) - \text{analytical } Y_1(x, t)}{\text{max.[analytical } Y_1(x, t)]}$$

over the rectangle $|x| \leqslant 10$, $t \leqslant 10$ was found to be 0.379%. This value compares unfavourably with the corresponding value 0.194% in Sozer & Greenberg (1993), but two points should be made. First, part of the error is due to the introduction of filtering here, filtering that is needed for stability. Secondly, a plot of the percent error, as a function of $x$ for $t = 2, 4, 6, 8, 10$, shows that the error is of a 'wavelet' form that moves outward with (but more slowly than) the overall wave system. Thus, it appears that the computed stagnation-point-type solutions are somewhat more accurate since they remain focused near the origin.

Turning to the supercritical case, consider a source flow for $F = \pm 2$. Numerical results are shown in figure 5, together with the one- and two-term perturbation solutions (denoted by ps1 and ps2, respectively), and they suggest that stable steady stagnation-point solutions exist beyond the critical value $F_{cr} \approx 1.42$ reported in Forbes & Hocking (1993) and Hocking & Forbes (1991). The numerical solution was less successful for sink flows, and even for large subcritical sink flows the calculations broke down so as to be inconclusive.

## 5. Finite-depth case

### 5.1. *Perturbation solution*

At steady state, we seek $Y(x) = FY_1(x) + F^2 Y_2(x) + \ldots$, and similarly for $G(x)$, $U(x)$, and $V(x)$. The evolution equations (2.1) and (2.2) give the coupled equations

$$F^1: \quad 0 = V_1, \tag{5.1a}$$

$$F^2: \quad 0 = V_2 - U_1 Y_{1x}, \tag{5.1b}$$

$$F^3: \quad 0 = V_3 - U_1 Y_{2x} - U_2 Y_{1x}, \tag{5.1c}$$

and

$$F^1: \quad 0 = Y_{1x}, \tag{5.1d}$$

$$F^2: \quad 0 = -(U_1 G_1)_x + \tfrac{1}{2}\kappa[-G_1 G_{1x} - 4U_1 U_{1x} - 4Y_{2x}], \tag{5.1e}$$

$$F^3: \quad 0 = -(U_1 G_2)_x - (U_2 G_1)_x + \tfrac{1}{2}\kappa[-G_1 G_{2x} - G_2 G_{1x} - 4U_1 U_{2x} - 4U_2 U_{1x} - 4U_1 V_{1x} Y_{1x} - 4Y_{3x}], \tag{5.1f}$$

respectively, and so on. The velocity terms in (5.1*a–f*) are

$$2\pi U_1(x) = \frac{x}{x^2+1} + \frac{x}{x^2+(2a-1)^2} + \int_{-\infty}^{\infty} \frac{2aG_1(\xi)}{(\xi-x)^2+4a^2}\,\mathrm{d}\xi, \tag{5.2a}$$

$$2\pi U_2(x) = -\frac{2xY_1(x)}{(x^2+1)^2} - \frac{2x(2a-1)\,Y_1(x)}{[x^2+(2a-1)^2]^2} + \int_{-\infty}^{\infty} \frac{2aG_2(\xi)}{(\xi-x)^2+4a^2}\,\mathrm{d}\xi + \int_{-\infty}^{\infty} \frac{2Y_1(x)\,G_1(\xi)}{(\xi-x)^2+4a^2}\,\mathrm{d}\xi - \int_{-\infty}^{\infty} \frac{16a^2 Y_1(x)\,G_1(\xi)}{[(\xi-x)^2+4a^2]^2}\,\mathrm{d}\xi, \tag{5.2b}$$

$$2\pi V_1(x) = \frac{1}{x^2+1} + \frac{2a-1}{x^2+(2a-1)^2} + \int_{-\infty}^{\infty} \left[-\frac{1}{\xi-x} + \frac{\xi-x}{(\xi-x)^2+4a^2}\right] G_1(\xi)\,\mathrm{d}\xi, \tag{5.2c}$$

$$2\pi V_2(x) = Y_1(x)\left\{\frac{1}{x^2+1} + \frac{1}{x^2+(2a-1)^2} - \frac{2}{(x^2+1)^2} - \frac{2(2a-1)^2}{[x^2+(2a-1)^2]^2}\right\} - \int_{-\infty}^{\infty} \frac{8aY_1(x)(\xi-x)\,G_1(\xi)}{[(\xi-x)^2+4a^2]^2}\,\mathrm{d}\xi - \int_{-\infty}^{\infty} \left[\frac{1}{\xi-x} - \frac{\xi-x}{(\xi-x)^2+4a^2}\right] G_2(\xi)\,\mathrm{d}\xi, \tag{5.2d}$$

and so on. Fourier transforming on $x$ is convenient owing to the convolution nature of the integrals, and leads to the steady-state solutions

$$G(x) = F\frac{1}{2a}\frac{\cosh(\pi x/2a)\sinh(\pi x/2a)}{\cosh^2(\pi x/2a) - \sin^2[\pi(a-1)/2a]} - F^2\frac{1}{2\pi a^{1/2}}\left(\frac{\kappa+1}{2\kappa}\right)^{1/2}\int_0^{\infty} \frac{1+\mathrm{e}^{-2aw}}{(1-\mathrm{e}^{-2aw})^2}\,wp(w)\sin(xw)\,\mathrm{d}w + O(F^3), \tag{5.3a}$$

$$Y(x) = FC_1 - F^2\left\{\frac{\kappa+1}{16a^2\kappa}\left[\frac{\cosh(\pi x/2a)\sinh(\pi x/2a)}{\cosh^2(\pi x/2a) - \sin^2[\pi(a-1)/2a]}\right]^2 + C_2\right\} + O(F^3), \tag{5.3b}$$

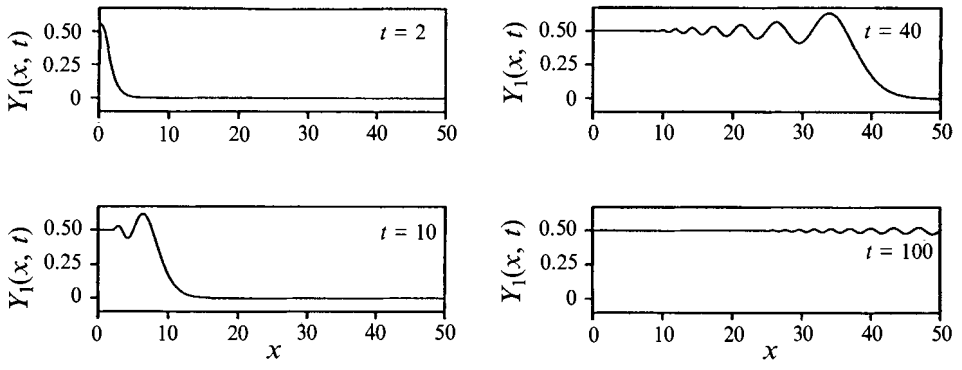


FIGURE 6. $Y_1(x,t)$ evolution for $\kappa = 1$; $a = 1$.

where $p(w) \equiv e^{-w} + e^{-w(2a-1)}$. The constants $C_1(\kappa, a)$ and $C_2(\kappa, a)$ cannot be found from (5.1). As seen from (5.3*a*, *b*),

$$G(x) \to F\frac{\operatorname{sgn}(x)}{2a} - F^2\frac{\operatorname{sgn}(x)}{4a^{5/2}}\left(\frac{\kappa+1}{2\kappa}\right)^{1/2} + O(F^3), \tag{5.4a}$$

and

$$Y(x) \to FC_1 - F^2\left[\frac{\kappa+1}{16a^2\kappa} + C_2\right] + O(F^3), \tag{5.4b}$$

as $x \to \infty$. We will refer to the latter as the 'setup/setdown' of the free surface at infinity for the source/sink flow in the presence of a finite depth flat bottom.

For the unsteady case, we seek $Y(x,t) = FY_1(x,t) + F^2Y_2(x,t) + \ldots$, and similarly for $G(x,t)$, $U(x,t)$, and $V(x,t)$. The non-dimensional source strength is $FH(t)$. The coupled equations for the leading terms $Y_1$ and $G_1$ are

$$F^1: \quad Y_{1t} = V_1,$$
$$F^1: \quad G_{1t} = -2\kappa(U_{1t} + Y_{1x}),$$

or

$$2\pi Y_{1t}(x,t) = H(t)\left[\frac{1}{x^2+1} + \frac{2a-1}{x^2+(2a-1)^2}\right] + \int_{-\infty}^{\infty}\left[-\frac{1}{\xi-x} + \frac{\xi-x}{(\xi-x)^2+4a^2}\right]G_1(\xi,t)\,\mathrm{d}\xi, \tag{5.5a}$$

$$\frac{\pi}{\kappa}G_{1t}(x,t) = -\delta(t)\left[\frac{x}{x^2+1} + \frac{x}{x^2+(2a-1)^2}\right] - 2\pi Y_{1x}(x,t) - 2a\int_{-\infty}^{\infty}\frac{G_{1t}(\xi,t)}{(\xi-x)^2+4a^2}\,\mathrm{d}\xi, \tag{5.5b}$$

where $\delta(t)$ is the Dirac delta function. Fourier transforming on $x$ and Laplace transforming on $t$ lead to the solution

$$G_1(x,t) = \frac{1}{\pi}\int_0^{\infty}\frac{p(w)\sin(xw)}{1-e^{-2aw}}\{1-[1+q(w)]\cos[t(wq(w))^{1/2}]\}\,\mathrm{d}w, \tag{5.6a}$$

$$Y_1(x,t) = \frac{1}{2\pi}\int_0^{\infty}\frac{p(w)\cos(xw)}{[wq(w)]^{1/2}}[1+q(w)]\sin[t(wq(w))^{1/2}]\,\mathrm{d}w, \tag{5.6b}$$

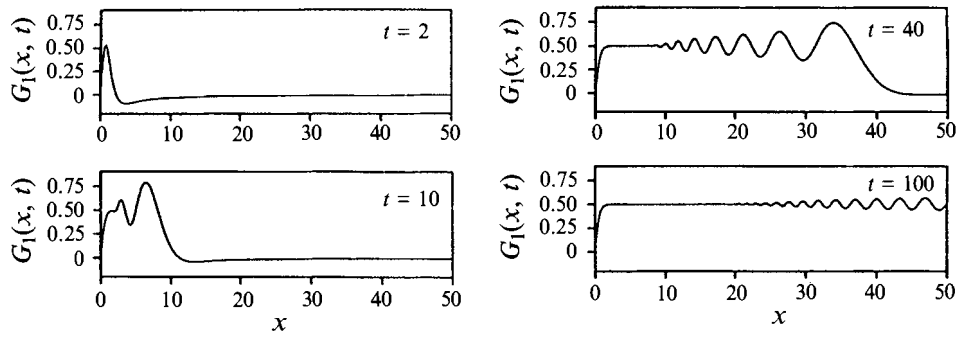


FIGURE 7. $G_1(x,t)$ evolution for $\kappa = 1$; $a = 1$.

where $p(w)$ is defined above and $q(w) \equiv \kappa(1-e^{-2aw})/(1+\kappa e^{-2aw})$. As $t \to \infty$, $Y_1(x,t) \to [(\kappa+1)/8a\kappa]^{1/2}$. Thus, $C_1 = [(\kappa+1)/8a\kappa]^{1/2}$ in (5.3*b*), but $C_2$ is still undetermined. Alternatively, $C_1$ could have been determined from the second-order terms in the steady-state mass flux condition

$$G(x)[a+Y(x)] = F/2 \tag{5.7}$$

as $x \to \infty$. However, (5.7) will not yield $C_2$ unless the $O(F^3)$ term in (5.4*a*) is known. For $\kappa = 1$ (i.e. zero air density) and $a = 1$ (i.e. the source or sink is at the bottom), $Y_1(x,t)$ and $G_1(x,t)$ are plotted in figures 6 and 7, respectively. Of course, $Y_1(x,t)$ and $G_1(x,t)$ are even and odd functions of $x$, respectively.

### 5.2. *Difference in steady state for source and sink*

As noted above, the literature on the submerged line source or sink in infinitely deep water has emphasized that the shape of the free surface, for steady stagnation-point-type flows, is insensitive to the sign of $F$. For the finite-depth case, however, our results in §5.3 show that the steady stagnation-point flows are similar, for sources and sinks, but not identical. Hocking & Forbes (1992) studied the finite-depth case, but did not consider this question since they focused on sink flows.

We have already seen in (5.3*b*) that $Y(x)$ is not an even function of $F$, if only because of the setup/setdown term $C_1 F$. However, it may be that all odd-order terms in (5.3*b*) are constants, so that $Y(x)$ would be insensitive to the sign of $F$, to within an additive constant setup/setdown. Thus, let us proceed one term further. Integrating (5.1*f*) on $x$ gives

$$Y_3 = -\left[\frac{1}{2\kappa}(U_1 G_2 + U_2 G_1) + \tfrac{1}{4} G_1 G_2 + U_1 U_2\right] + C_3, \tag{5.8}$$

where $U_1$, $U_2$ are given in (5.2*a*, *b*) and $G_1$, $G_2$ are given in (5.3*a*). It is easily seen from (5.8) that $Y_3(x)$ is not a constant since $Y_3(0) = C_3$, whereas

$$Y_3(x) \to \frac{1}{16\sqrt{2}a^{7/2}}\left(\frac{\kappa+1}{\kappa}\right)^{3/2} + C_3$$

as $x \to \infty$. Thus, for the finite-depth case the free surface elevation for steady stagnation-point flows differs for sources and sinks not only in the presence of a finite setup/setdown but also in its shape as well.

### 5.3. *Numerical results*

In the finite-depth case the wave front propagates more slowly than in the infinite-depth case, so that a smaller computational domain is possible. Guided by figures 6 and 7, we chose the computational domain to be $-80 < x < 80$, so that we could carry the

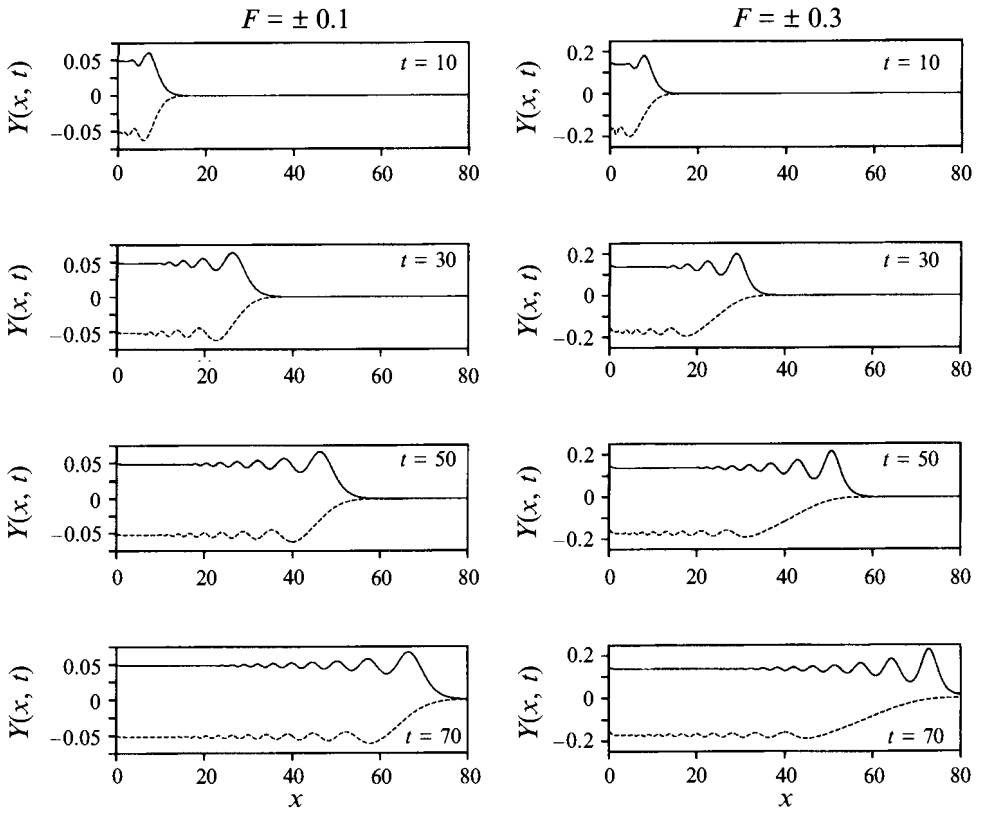


FIGURE 8. $Y(x, t)$ evolution for $F = \pm 0.1$, $F = \pm 0.3$; solid line for source, dashed for sink.

solution as far as $t = 70$. However, the advantage of a smaller computational domain was offset by a considerable reduction in the speed of convergence of the iterations present in the time integrations. This reduction was noted in Baker *et al.* (1982) as well.

The cases $F = \pm 0.1$ were run for $\kappa = 1$ and $a = 1$ and results are shown in figures 8 and 9. $F = \pm 0.1$ is not so small for the finite-depth case since stagnation-point solutions have been reported only for $|F| < F_{cr} \approx 0.23$ for $a = 1$ (Hocking & Forbes 1992). Figures 8 and 9 indicate an approach to a steady stagnation-point flow. We would like to compare that result with the steady state $Y(x) \approx FY_1(x) + F^2Y_2(x) + F^3Y_3(x)$ given by (5.3*b*) and (5.8), but we do not know $C_2$ or $C_3$. To at least be able to compare the shape of the three-term steady-state solution $Y(x)$ (i.e. up to $O(F^3)$ with that of the computed solution $Y(x, 70)$, we have arbitrarily adjusted $-F^2C_2 + F^3C_3$ so as to fit the two solutions near $x = 4$, at $t = 70$, and have displayed the three-term steady-state solution as open squares in figure 9.

The supercritical cases $F = \pm 0.3$ were also run. The source and sink generate somewhat different $Y(x, t)$ even at steady state (figures 8 and 9). Figures 8 and 9 strongly suggest an approach to steady state.

Finally, we note that the speed of propagation of the leading wave crest of $Y(x, t)$ was calculated to be roughly 1.0, 0.9, 1.1, 0.7 for $F = +0.1$, $-0.1$, $+0.3$, $-0.3$, respectively, whereas the speed predicted by the linear shallow-water theory, namely $a^{1/2}$ (or, in dimensional form, $(gD)^{1/2}$) is unity.

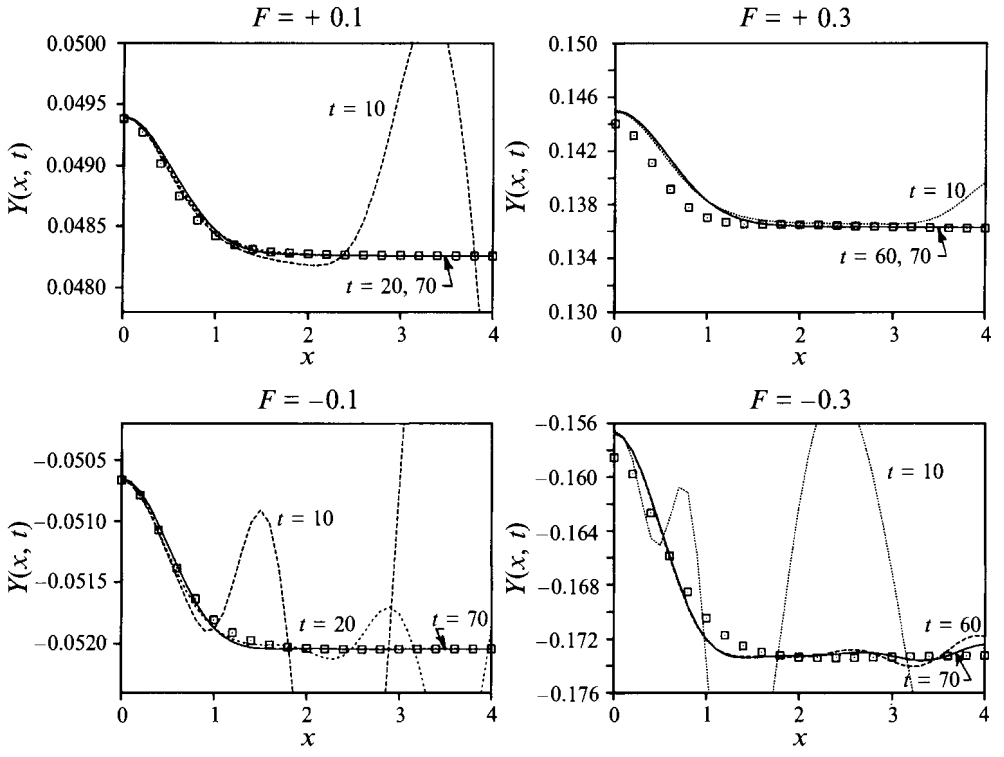


FIGURE 9. Blow-up of $Y(x,t)$ for $F = \pm 0.1$ and $F = \pm 0.3$. Open squares denote three-term steady-state perturbation solution.

## 6. Discussion and conclusions

The Zaroodny/Greenberg evolution equations were used to obtain both numerical solutions and perturbation solutions in the Froude number for the flow induced by a line source or sink lying between a free surface and a flat bottom. Whereas numerous investigators have studied the steady-state problem, the present paper has emphasized the unsteady flow and approach to steady state.

For the infinite-depth limit, an approach to a steady stagnation-point flow was found for subcritical (i.e. for $F$ smaller than the critical value 1.42 cited in the literature) source flows and sufficiently subcritical sink flows, and for supercritical source flows. For the finite-depth case, an approach to a steady stagnation-point solution was found for subcritical and supercritical sink flows and for source flows. In addition, a finite free surface setup/setdown of $F[(\kappa+1)/8a\kappa]^{1/2} + O(F^2)$ was found, due to the finite depth, from either the first-order unsteady problem or from the second-order steady-state mass flux condition (5.7). Besides this finite setup/setdown, it was shown that the shape of the free surface also differs for source and sink flows.

## REFERENCES

ABRAMOWITZ, M. & STEGUN, I. A. 1964 *Handbook of Mathematical Functions*. Washington: US Govt. Printing Office.

BAKER, G. R., MEIRON D. I. & ORSZAG, S. A. 1982 Generalized vortex methods for free surface problems. *J. Fluid Mech.* **123**, 477–501.

CRAYA, A. 1949 Theoretical research on the flow of nonhomogeneous fluids. *La Houille Blanche* **4**, 44–55.

FORBES, L. K. & HOCKING, G. C. 1993 Flow induced by a line sink in a quiescent fluid with surface-tension effects. *J. Austral. Math. Soc.* B **34**, 377–391.

HOCKING, G. C. 1985 Cusp-like free-surface flows due to a submerged source or sink in the presence of a flat or sloping bottom. *J. Austral. Math. Soc.* B **26**, 470–486.

HOCKING, G. C. 1991 Critical withdrawal from a two-layer fluid through a line sink. *J. Engng Maths* **25**, 1–11.

HOCKING, G. C. & FORBES, L. K. 1991 A note on the flow induced by a line sink beneath a free surface. *J. Austral. Math. Soc.* B **32**, 251–260.

HOCKING, G. C. & FORBES, L. K. 1992 Subcritical free-surface flows caused by a line source in a fluid of finite depth. *J. Engng Maths* **26**, 455–466.

LONGUET-HIGGINS, M. S. & COKELET, E. D. 1976 The deformation of steep surface waves. I. A numerical method of computation. *Proc. R. Soc. Lond.* A **350**, 1–26.

PEREGRINE, D. H. 1972 A line source beneath a free surface. *Mathematics Research Center, Univ. Wisconsin Rep.* 1248.

SHAPIRO, R. 1975 Linear filtering. *Maths Comput.* **29**, 1094–1097.

SOZER, E. M. 1994 Vortex sheet approach to the nonlinear flow induced by a moving object below a free surface. (tentative title) PhD dissertation, Mech. Eng. Dept. University of Delaware.

SOZER, E. M. & GREENBERG, M. D. 1993 A vortex sheet approach to the nonlinear flow induced by a line soure or sink. In *Boundary Elements XV, Proc. 15th Intl Conf. on BEM* (ed. C. A. Brebbia & J. J. Rencis). Elsevier.

TELSTE, J. G. 1987 Inviscid flow about a cylinder rising to a free surface. *J. Fluid Mech.* **182**, 149–168.

TUCK, E. O. & VANDEN-BROECK, J. M. 1984 A cusp-like free-surface flow due to a submerged source or sink. *J. Austral. Math. Soc.* B **25**, 443–450.

VANDEN-BROECK, J. M. & KELLER, J. B. 1987 Free surface flow due to a sink. *J. Fluid Mech.* **175**, 109–117.

VANDEN-BROECK, J. M., SCHWARTZ, L. W. & TUCK, E. O. 1978 Divergent low-Froude number series expansion of nonlinear free-surface problems. *Proc. R. Soc. Lond.* A **361**, 207–224.

ZAROODNY, S. J. & GREENBERG, M. D. 1973 On a vortex sheet approach to the numerical calculation of water waves. *J. Comput. Phys.* **11**, 440–446.